Article:

Du, H, Xu, Z, Hu, M et al. (7 more authors) (2020) Natural organic matter decreases uptake of W(VI), and reduces W(VI) to W(V), during adsorption to ferrihydrite. Chemical Geology, 540. 119567. ISSN 0009-2541

https://doi.org/10.1016/j.chemgeo.2020.119567

Natural organic matter decreases uptake of W(VI), and reduces W(VI) to W(V), during adsorption to ferrihydrite

Huihui Du,[1, 2] * Zelin Xu,[1] Meng Hu,[1] Huanjing Zhang,[1] Caroline L. Peacock,[3] Xin Liu,[1, 2] Ning Nie,[1, 2] Qin Xue,[1] Ming Lei,[1, 2] Boqing Tie,[1, 2]

[1] Hunan Engineering & Technology Research Center for Irrigation Water Purification, College of Resources and Environment, Hunan Agricultural University, Changsha 410128, People's Republic of China

[2] Key Laboratory of Southern Farmland Pollution Prevention and Control, Ministry of Agriculture, Changsha 410128, People's Republic of China

[3]School of Earth and Environment, University of Leeds, Leeds, LS2 9JT, UK

*Corresponding Author: **Huihui Du** (Dr.)

E-mail: duhuihui@hunau.edu.cn; duhuihui@webmail.hzau.edu.cn

Address: 1st Nongda Road, Furong district, Changsha City, China.

Abstract

Tungsten is both naturally occurring and an anthropogenically released contaminant metal in soils, sediments and water systems that typically exits as the soluble tungstate oxyanions, $W(VI)O_4^{2-}$. Tungsten mobility and fate are strongly dependent on the adsorption of tungstate to mineral surfaces. However, environmental mineral surfaces are commonly coated with natural organic matter (NOM), and the role of this coating in the tungsten adsorption process, and thus in controlling tungsten reactivity and transport, is unclear. This study investigates W(VI) adsorption to ferrihydrite (Fh), a ubiquitous iron (hydr)oxide in soils and sediments, both in the absence and presence of humic acid (HA), a widely occurring type of NOM, using batch experiments coupled with spectroscopic and thermodynamic techniques. Kinetic results indicate that access to the adsorption sites for W(VI) on the organomineral surfaces is limited when Fh is coprecipitated with HA. Commensurate with this observation, batch experiments show that HA decreases W(VI) adsorption to Fh over a wide pH range (4-11), and this inhibitory effect is more pronounced at higher HA concentration. X-ray photoelectron spectroscopy (XPS) measurements demonstrate the formation of inner-sphere type W complexes on both the Fh and HA fraction of the Fh-HA binary composite. In particular, ~40% of the adsorbed W(VI) species is reduced to W(V) in the presence of HA. Attenuated total reflectance Fourier transform infrared spectroscopy (ATR-FTIR) results show the presence of poly tungstate species on Fh, particularly at lower pH and in the presence of HA. Isothermal titration calorimetry shows that W(VI) adsorption to Fh is an exothermic process both in the presence and absence of HA, and that process is accompanied by a positive entropy. The findings of this work suggest that NOM not only mobilizes tungstate but also reduces tungstate from W(VI) to W(V) at environmental iron (hydr)oxide-water interfaces, which is of significance for evaluating the migration and bioavailability of tungsten in both natural and contaminated environments.

Keywords: tungsten, adsorption, iron (hydr)oxide, NOM, organo-mineral association, tungsten reduction, isothermal titration calorimetry

1. Introduction

Tungsten (W) is both a naturally occurring element and an anthropogenic contaminant, that is increasingly released into the environment as a result of its use in a wide range of industrial products that require high heat resistance and mechanical toughness, such as light bulbs, bullets and many metal alloy (Koutsospyros et al., 2006). Recent reports of W contamination in groundwater and soil systems have raised concerns about its potential toxicity to plants, animals and humans (Kennedy et al., 2012; Tuna et al., 2012; Datta et al., 2017; Lindsay et al., 2017; Mohajerin et al., 2014a; 2014b; Oburger et al., 2018), and because of its risk to natural systems, W has been listed as an emerging contaminant by the United States Environmental Protection Agency (EPA) (https://www.epa.gov/fedfac/technical-fact-sheet-tungsten). Despite its listed status however, the biogeochemical behavior and potential risks of W to human and environmental health are still poorly understood.

Metallic W is generally insoluble with little or no mobility, however, under near-surface conditions W is present in an oxidized state, and forms a variety of oxyanionic species, such as the W(VI) species tungstate WO_4^{2-} and poly tungstate $W_7O_{24}^{6-}$, which dissolve in water and are mobile in the environment (Dermatas et al., 2004; Clausen and Korte, 2009). When W is present as dissolved tungstate oxyanions (e.g., WO_4^{2-}), strong uptake may occur at mineral-water interfaces, influencing its mobility and fate in soils, sediments and water systems (Johannesson et al., 2013). Recently, iron-bearing minerals such as ferrihydrite, hematite, goethite, iowaite and pyrite have been reported as an important sink for tungstate oxyanionic species (Gustafsson, 2003; Cui and Johannesson, 2017; Iwai and Hashimoto, 2017; Rakshit et al., 2017; Sallman et al., 2018; Cao et al., 2019). For example, iowaite, an iron-bearing layered double hydroxide $[Mg_6Fe_2(OH)_{16}Cl_2 \cdot 4H_2O]$, can sorb up to 71.9 mg/g tungstate from aqueous solution (Cao et al., 2019). In general, tungstate adsorption increases with decreasing pH (Gustafsson, 2003; Cui and Johannesson, 2017; Sallman et al., 2018), and spectroscopic measurements, such as those made using attenuated total reflectance Fourier transform infrared spectroscopy (ATR-FTIR) and X-ray absorption spectroscopy (XAS), demonstrate the formation of inner-sphere type adsorption complexes during tungstate binding to iron (hydr)oxides including ferrihydrite and hematite (Sun and Bostick, 2015; Rakshit et al., 2017; Sallman et al., 2018), and the strength of this interaction is greater with decreasing pH. Tungsten oxyanions can also polymerize to form poly tungstate species (Strigul et al., 2009; Strigul, 2010), which can decrease tungstate adsorption onto ferrihydrite (Gustaffson, 2003), thereby potentially mobilizing W in the environment (Bostick et al., 2018). Of particular relevance to natural systems, competing oxyanions such phosphate (P) can inhibit the retention of tungstate on hematite (Sallman et al., 2018), and the surface complexation of tungstate in the competitive system differs from that in the absence of PO_4^{3-}. This indicates that moieties that compete with tungstate for available sorption sites on iron (hydr)oxides are able to significantly modify W mobility and fate in soils and sediments.

One such competing moiety that is widely distributed in soils, sediments and water systems is natural organic matter (NOM). This is known to bind strongly with iron (hydr)oxides via surface adsorption and/or (Sposito, 1984; Chen et al., 2014; Kleber, 2015). These processes result in the formation of an organo-mineral composite (Kleber et al., 2015), in which surface properties are quite different from those of pure iron (hydr)oxide, thereby potentially affecting the transport and eventual fate of trace elements (Moon and Peacock, 2012; Liang et al., 2013; Seda et al., 2016; Du et al., 2016; Wang et al., 2016; Flynn and Catalano, 2017; Otero-Fariña et al., 2017; Du et al., 2018a; 2018b; Fariña et al., 2018; Woodward et al., 2018; Xue et al., 2019). However, whether and to what extent NOM affects the binding of soluble tungstate oxyanions to mineral surfaces is still unknown. Moreover, W has several oxidation states (+4 ~ +6), and whether oxidation-reduction occurs in the presence of NOM is unclear. This fundamental information is vital to understand the controls on tungstate mobility, bioavailability and toxicity in natural systems.

The purpose of this study was to examine the influences of NOM, represented by the widely abundant organic moiety humic acid (HA), on tungstate adsorption and oxidation/reduction at typical iron (hydr)oxide-water interfaces. By varying total W concentration, pH or equilibration time, a variety of experimental analogues were investigated to simulate complex natural systems. In addition, the structures of adsorbed W species and the thermodynamic binding properties were also investigated using X-ray photoelectron spectroscopy (XPS), attenuated total reflection Fourier transform infrared spectroscopy (ATR-FTIR) and isothermal titration calorimetry (ITC). Two different NOM concentrations were also considered, which represent either OM poor or rich environments. Our results shed new light on the role of NOM in tungstate adsorption and valence state changes at typical mineral-water interfaces. Such information is required to accurately predict the mobility and thus eventual fate of W in natural soils, sediments and water systems.

2. Experimental methods

All chemicals and reagents used were of analytical grade. All solutions were made with ultrapure water (18.2 MΩ·cm). The W(VI) stock solution was prepared from sodium tungstate dihydrate ($Na_2WO_4 \cdot 2H_2O$). The background electrolyte was sodium chloride (NaCl) prepared at 0.01 M. Plastic labware was used throughout the experiments and cleaned with dilute nitric acid before use.

2.1 Synthesis of ferrihydrite and ferrihydrite-HA binary composite

A commercial peat-derived HA (No: H16752, Sigma-Aldrich (Shanghai) Trading Co.Ltd., China) was selected as an analogue for natural organic matter, and purified followed the protocols of Du et al. (2016). Pure ferrihydrite (Fh) was synthesized by hydrolysis of a 0.1 M Fe^{3+} salt solution to pH ~7.5 with NaOH. For preparation of the Fh-HA binary composite, 0.1 M Fe^{3+} salt solution was first reacted with two known amounts of HA solution for 2 h, generating C/Fe molar of 0.47 and 2.33, respectively, then subjected to a base hydrolysis to pH ~7.5. These preparations resulted in Fh-HA composites with approximately 5 wt% and 15 wt% C (Du et al., 2018b), and were abbreviated as FhHA_5%C and FhHA_15%C, respectively. Both pure Fh and Fh-HA composite were rinsed several times until no dissolved organic carbon (DOC) was detected in the supernatant liquid (Du et al., 2018b).

2.2 W(VI) adsorption experiments

Adsorption experiments were performed in batch systems at room temperature (~25°C). In each centrifuge tube, a mixed solution (~30 mL) contained known amounts of adsorbent (Fh or Fh-HA, 0.05 g/L), W(VI) and background electrolyte (0.01 M NaCl). For adsorption kinetics, the initial concentration of W(VI) was fixed at ~0.165 mmol/L (~30 mg/L), and the pH was controlled at pH 6.5. During the kinetic experiments, an aliquot of adsorption suspension (~1 mL) was taken successively by pipette at 1, 5, 15, 25, 50, 150, 300 and 900 min intervals. For adsorption edge experiments (pH 4-11), the initial concentration of W(VI) was fixed at ~0.165 mmol/L, and the pH was adjusted to the target pH using dilute HNO_3 or NaOH. For adsorption isotherms experiments (pH 6.5 as a representative) experiments, the concentration of W(VI) was varied from 0 to ~0.43 mmol/L. Centrifuge tubes for adsorption edges and isotherms were lightly shaken continuously for ~15 h to reach equilibrium. The suspensions were then centrifuged and filtered through 0.22 μm membrane filters and 3k Dalton ultrafilters (Du et al., 2018b). The W(VI) concentration was measured using ICP-OES (PerkinElmer Optima 8300) and the supernatant thick paste was recovered for XPS analyses. All adsorption experiments were performed in duplicate.

2.3 XPS experiments

The residual thick pastes left in the adsorption experiments were freeze-dried and ground into powder samples, then sealed in polyethylene bags for XPS analysis. Spectra of W 4f (5p), O 1s and C 1s were measured using the KRATOS Axis Ultra X-ray photoelectron spectrometer (Thermo Fisher Scientific, US) equipped with a monochromatic Al Kα source and a charge compensation system. During data collection, the step size was 0.05 eV, and 10 scans for each sample were averaged. For XPS analyses, the C 1s peak at ~284.8 eV was used to calibrate the binding energy, and the curve-fitting program XPSPEAK41 was used to fit the spectra (Xue et al., 2019).

2.4 In situ ATR-FTIR experiments

In situ ATR-FTIR experiments were performed on a PerkinElmer FT-IR spectrometer equipped with an advanced 6 reflection ATR system (ZnSe crystal, 45° angle) for the infrared analysis of liquids and pastes. The flow cell consists of a rectangular holder coated with a thin film of either Fh or Fh-HA, prepared by overnight drying of 1 mL of suspension evenly spread across the crystal surface. Background electrolyte (0.01 M

NaCl) was first pumped through the reaction vessel at a rate 1 mL/ min, until the IR signals were no longer increasing. Then a freshly prepared W(VI) stock solution was introduced through the flow cell, and the spectra were recorded every 40 min, until the IR signals were no longer increasing. The characteristic IR absorbances of adsorbed W species were predominately in the range of 1400 to 700 cm^{-1} (Rakshit et al., 2017). All experiments were conducted at pH 4.5, 6.5 and 8.5.

2.5 ITC experiments

Adsorption calorimetry was conducted using a TAM III thermal activity monitor system (TA Instruments, US) equipped with a 1 mL reaction cell and a 500 μL micro-syringe. Prior to measurements, 0.7 mL of sorbent solution (5 g/L) was placed in the reaction cell string at 120 rev min^{-1}. The sample was left to stabilize to achieve a highly stable heat flow (i.e., a signal excursion < 250 nw/hr). The W(VI) solution (~5.44 mmol/L) was subsequently titrated into the sorbent solution at a rate of 1 μL/s, and the adsorption heat flow (μW) was recorded continuously. Each titration was 10 μL with an interval of 600 s. A control experiment was conducted by titrating W(VI) solution into the background electrolyte to exclude the dilution heat that was not caused by W(VI) adsorption. All measurements were performed at pH 6.5 and 298 K. Data processing was accomplished using the software TAM assistant (ver. 1.4) and NanoAnalyze (ver. 3.6, TA Instruments, US) for the determination of ΔG, ΔH, ΔS and binding affinity (K) (Du et al., 2018c; 2019). The experimental ITC data were fit by an independent-site model (dotted lines in Fig. 6) described in Freire et al. (1990):

$$Q = V[\mathrm{M}]\frac{\mathrm{n}\Delta HK[\mathrm{L}]}{1+K[\mathrm{L}]}$$

where V is the volume of the reactor, ΔH is enthalpy (kJ/mol), K (M^{-1}) represents the thermodynamic affinity, [L] is the total W concentration, [M] is the sorbent concentration, and n is the number of binding sites. The Gibbs free energy (ΔG) was calculated by: $\Delta G = -R\mathrm{T}\ln \mathrm{K}_a$, where R = 8.314 J/mol/K, T = 298 K. The entropy change ΔS was calculated by: $\Delta S = (\Delta H - \Delta G)/\mathrm{T}$.

3. Results

3.1 Macroscopic adsorption phenomena

Tungstate adsorption kinetics are investigated to explore whether the presence of HA affects the W(VI) adsorption rate onto Fh surfaces, and the results are shown in Figure. S1. The plots represent the adsorbed amount of W(VI) (mmol/kg) plotted against time (h). For all the systems studied, a two-stage kinetic behavior is apparent: a fast initial adsorption in the first 1 h, followed by a slow adsorption, and it is apparent that after 3 h reaction W(VI) adsorption reaches equilibrium. Herein, a Pseudo-second order model (solid lines in Fig. S1) provides a good fit to the data (≥0.92), and is used to obtain the kinetic adsorption parameters. This model has been widely used in describing the kinetics of metal adsorption to a variety of sorbents (Zhu et al., 2011; Du et al., 2017; Yan et al., 2017). The Pseudo-second order model can be expressed as: $1/(q_e - q_t) = 1/q_e + kt$, where q_e is the equilibrium adsorption amount and k represents the rate constant. The model fits in Figure. S1 show that W(VI) adsorption rates on different sorbents follow the order Fh (19.9) > FhHA_5 wt% C (17.3) > FhHA_15 wt% C (11.5). This observation shows that the W(VI) adsorption rate decreases for increasingly organic-rich minerals, and suggests that access to the adsorption sites on the organomineral surfaces is limited when Fh is coprecipitated with NOM.

Tungstate adsorption edge results are shown in Figure. 1. Over a wide pH range from 4 to 11, W(VI) adsorption decreases with increasing pH, in agreement with W(VI) adsorption trends observed for other mineral sorbent systems such as hematite (Sallman et al., 2018), birnessite, gibbsite, goethite, montmorillonite (Iwai and Hashimoto, 2017), boehmite (Hur and Reeder, 2016), iowaite (Cao et al., 2019) and pyrite (Cui et al., 2017). A reverse adsorption edge is expected for adsorption of W(VI) oxyanionic species on Fh, as with a pH_{pzc} between 7-9 (Schwertmann and Fechter, 1989). The surface adsorption sites become increasingly negatively charged with increasing pH, therefore increasing the repulsive force between the adsorbing ions and the mineral surface. Results show that humic acid inhibits the adsorption of W(VI) to Fh, and the inhibitory effect of HA increases with increasing HA concentration. This phenomenon is reported for the adsorption of metal cations onto iron (hydr)oxide organominerals (Moon and Peacock, 2012; Du et al., 2016; 2018a; 2018b; Otero-Fariña et al., 2017; Woodward et al., 2018), but is less commonly investigated for oxyanions (Xue et al., 2019).

Tungstate adsorption isotherms are adequately described by the Langmuir model (R^2 values≥0.92) (Fig. 2, Table S1). The Langmuir parameter $Q_{\max}$ (mmol/kg) is the maximum adsorption capacity; K (L/mol) is the binding energy constant, and greater K values indicate a higher affinity between W(VI) and the sorbent (Sparks, 2002). Results show that the Fh-HA binary composites have lower $Q_{\max}$ tungstate adsorption capacities

(857-1272 mmol/kg) than pure Fh (1847 mmol/kg) and moreover, that the binding affinities (*K*) for W(VI) adsorption to the Fh-HA binary composites are lower than that for pure Fh (Table S1). These two aspects together indicate that increasing concentrations of NOM associated with iron (hydr)oxide increasingly inhibit W(VI) adsorption to organomineral surfaces.

3.2 Molecular W(VI) adsorption characteristics

X-ray photoelectron spectroscopy is a powerful surface analysis technique, providing valuable information about the elemental composition and local chemical environments of adsorbed species, and therefore offers W(VI) molecular binding information for W(VI) adsorption on Fh and Fh-HA surfaces. Figure 3 shows the O 1s XPS spectra of the Fh and Fh-HA composite before and after the adsorption of W(VI). In general, the O 1s peaks at ~531 eV become broader after the binding of W(VI) for both the Fh and Fh-HA composite. The O region can be decomposed into three components: oxygen in the crystal lattice of Fh (Fe-$\underline{O}$-Fe), ~530 eV; oxygen on the surface of Fh, ~531 eV, and oxygen in the adsorbed water molecules, 532.6 eV (Xue et al., 2019). For pure Fh, the component at ~531 eV increases from ~29% to ~40% after W(VI) adsorption; for the Fh-HA binary composite, this increment is ~9%. These spectral changes suggest that the surface hydroxyl groups of the Fh and Fh-HA composite interact with the W(VI) oxyanion species, likely forming inner-sphere type complexes in which one or more of the O atoms in the W(VI) oxyanion are exchanged with O atoms of Fe-OH surface adsorption sites. Using EXAFS, similar inner-sphere type adsorption complexes on boehmite (γ-AlOOH) were also found by Hur and Reeder, (2016; 2018). The smaller increase in the ~531 eV component before and after adsorption for the Fh-HA binary composite is likely due to the smaller amount of W(VI) adsorbed to the composite, compared to Fh, as observed in the batch adsorption results above.

The W (4f, 5p) higher resolution XPS spectra in Figure. 4 also clearly show the presence of W associated with the Fh and Fh-HA composite after adsorption, and the peak intensity is more pronounced for pure Fh (blue line), which again agrees with the smaller amount of W(VI) adsorbed to the composite, compared to Fh. Importantly, the W $4f_{5/2}$ and W $4f/_{7/2}$ peak binding energies shift from 37.9 eV and 35.6 eV for the W-loaded Fh to 37.6 eV and 35.0 eV for the W-loaded Fh-HA, respectively. These observations suggest that the oxidation state of some proportion of the adsorbed W(VI) is reduced during binding to the Fh-HA composite. In order to evaluate the contribution of oxidized W(VI) and reduced W to the total adsorption, a typical peak (W $4f_{7/2}$, 34-37 eV) for W-loaded Fh-HA can be decomposed and fitted into two peaks (Fig. 4): one located at ~35.0 eV, which is assigned to W^{6+}, accounting for ~60% of the total adsorbed W, and one located at ~35.6 eV, corresponding to W^{5+}, and accounting for ~40% of the total adsorbed W species (Xie et al., 2012; Yang et al., 2018). Results therefore suggest that the presence of NOM at iron (hydr)oxide surfaces reduces a significant proportion of W(VI) to W(V) during adsorption.

To investigate whether complexation occurs between the HA fraction of the Fh-HA composites and W oxyanions. The C 1s XPS peaks (Fig. S2) can be decomposed into three components, C_xH_y (~284.6 eV), C-O (~286.0 eV) and COO (~288.5 eV)

(Schild and Marquardt Christian, 2000). Results show an increase of the C-O fraction from 9.4% to 24.6% after the adsorption of W(VI). This increased peak intensity suggests there is complexation between W and HA, such that this new species contributes to the C-O peak intensity. Overall, our W and C XPS results show that W oxyanions form complexes with both the Fh and HA adsorption sites present in the Fh-HA binary composite, and this process is also accompanied by the reduction of ~40% of the W(VI) to W(V).

Attenuated total reflection Fourier transform infrared spectra were also adopted to further evaluate the molecular interaction of W(VI) with the Fh and Fh-HA composite (15 wt% C) at different pHs 4.5, 6.5 and 8.5. The most characteristic peaks for adsorbed W species occur between 700~1000 cm^{-1} (Sallman et al., 2018). As shown in Figure. 5, one strong peak at ~930 cm^{-1} and one broad peak at 810 cm^{-1} are observed, corresponding to the symmetric and antisymmetric stretching modes of W−O vibrations, respectively (Sallman et al., 2018). This confirms that the adsorption of W on Fh and Fh-HA surfaces occurs via a strong inner-sphere type surface complexation of W(VI) with surface O atoms. The band intensities increase with decreasing pH, owing to the decreased amount of W adsorbed However, the spectra show some changes in the shape of the IR peak at ~810 cm^{-1} (Fig. 5). Specifically, for W-adsorbed Fh samples at pH 6.5 and 4.5, and all W-adsorbed Fh-HA composite samples, the IR peak broadens towards higher frequencies. Interestingly, the W−O−W stretching vibrations, which are characteristic of polymeric tungstate species can appear at ~860−880 cm^{-1} (Davantès et al., 2016; Rakshit et al., 2017; Tribalis et al., 2014). Results therefore suggest the presnece of poly tungstate species on Fh and Fh-HA at pH≤6.5. Moreover, the polymerization appears to be more pronounced at lower pH and in the presence of NOM, as evident from the spectra differences in Figure 5.

3.3 Thermodynamic adsorption characteristics

To gain a deeper insight into the fundamental driving mechanisms for W adsorption, ITC was performed to obtain the thermodynamic parameters describing W(VI) adsorption on the Fh and Fh-HA composite. Figure 6 shows that W(VI) adsorption onto the both Fh and Fh-HA composite is an exothermic process. The peak amplitudes and areas gradually decrease as more W(VI) is added, most likely due to a decrease of available adsorption sites as added W(VI) is taken up. The adsorption trend of W(VI) on pure Fh is strikingly different from those on the Fh-HA composite. For pure Fh, continued releases of heat are detected for the first 10 injections, after which there is a relatively gradual decline; for FhHA_5%C, the first 5 injections produce comparable amounts of heat, but then heat flow decreases sharply; while for FhHA_15%C, the released heats decrease almost linearly over the whole titration period. Moreover, the total heat produced follows the order of Fh > FhHA_5%C > FhHA_15%C. These observations corroborate the batch adsorption, spectroscopic and thermodynamic results, that more W(VI) is adsorbed on pure Fh than on Fh-HA composites

The Gibbs free energy (ranges from -20.64 to -14.31 kJ/mol) in Table 1 shows that the binding of W(VI) on the Fh and Fh-HA composites is a spontaneous process ($\Delta G < 0$), particularly for pure Fh. Moreover, the K_a values imply that pure Fh exhibits a higher affinity for W(VI) than Fh-HA binary composites. When looking at the enthalpy, results show that W-Fh interaction gives rise to a larger enthalpy change (16.1 kJ/mol) compared to the W-Fh-HA interactions (10.2-15.43 kJ/mol). These findings also corroborate that W(VI) adsorption is suppressed in the presence of HA. The entropy changes (ΔS) can further provide information on the coordination environments of the adsorbed W oxyanions, i.e., inner-sphere complex formation commonly generates a positive ΔS while outer-sphere complex formation produces a negative ΔS because the former displaces solvating water molecules from the adsorption coordination sites, whereas the latter does not (Nancollas, 1970; Gorman-Lewis et al., 2006; Du et al., 2017). Our ΔS data (12.96-15.03 J/mol/K) therefore provide clear evidences for the formation of inner-sphere type of W species on Fh and Fh-HA surfaces.

4. Discussion

Adsorption onto mineral surfaces is an important process controlling tungsten mobility and thus the eventual fate of natural and anthropogenic tungsten in soils, sediments and aquatic systems. However, the ubiquitous existence of natural organic matter (NOM) is known to significantly influence the adsorption process of many metals because NOM strongly interacts with mineral phases, giving rise to a change in the mineral surface charge and/or number and type of reactive surface adsorption sites, and thus the interaction of mineral surfaces with natural and contaminant metals. This study represents a scenario in which tungstate oxyanion species occur in natural environments where iron (hydr)oxides are associated with NOM. Results show, for the first time, that the presence of NOM coprecipitated with iron (hydr)oxide at environmentally representative concentrations of NOM (~5 wt% and 15 wt% OC) inhibits the adsorption of W(VI) to the resulting organominerals over a wide pH range (4-11) at both environmentally representative (~5 wt% OC) and high level (15 wt% OC) of NOM. In this way, natural organic matter can act to increase the mobility of tungsten in the environment. Several explanations for this phenomenon are possible, notably: 1) it is well known that NOM can decrease the specific surface area and pore volume of Fh (Mikutta et al., 2014), which likely reduces the number and density of surface adsorption sites available for tungsten uptake; 2) it is also observed that NOM can competitively adsorb to iron (hydr)oxides via ligand exchange of the carboxylic and phenolic functional groups with Fe-OH (Du et al., 2018b; Oren and Chefetz, 2012; Chen et al., 2014; Mikutta et al., 2014), thus reducing the number of surface adsorption sites available for tungsten uptake; 3) the Fh surface is known to undergo changes in surface charge (Moon and Peacock, 2012; Du et al., 2018a, b), and in particular the pH_{PZC} is known to significantly reduce such that the surface adsorption sites become more negatively charged when coated with NOM (Xue et al., 2019), which likely enhances electrostatic repulsion between tungstate oxyanions and surface adsorption sites; and 4) results here show that NOM promotes the formation of poly tungstate species(shown in ATR-FTIR) which have a lower affinity towards the adsorbent surfaces (Sun and Bostick, 2015). It is notable that the inhibitory effect of NOM on W(VI) adsorption is not equal over the whole pH range, and instead decreases with increasing pH. This can be explained by that fact that NOM binding to iron (hydr)oxide is strongly pH dependent, with favorable adsorption at acidic or slightly acidic pH conditions (Davis, 1982; Murphy et al., 1992; Gu et al., 1994). With increasing pH, the binding affinity between NOM and iron (hydr)oxide decreases, and as such the inhibitory effect, as a result of the four reasons outlined above, also decreases. Moreover, our ATR-FTIR results show clearly the presence of polymeric tungstate species on Fh surfaces, in particular at pH 4.5. And also because polymeric tungstate species have lower adsorption affinities for mineral surfaces than tungstate monomers (Sun and Bostick, 2015), therefore, the inhibitory effect of NOM on W(VI) adsorption is more pronounced at lower pH.

Natural organic matter in the form of humic acid not only inhibits the retention of tungstate to Fh, but also results in the reduction of a significant proportion (~40%) of adsorbed W(VI) to W(V). This reductive phenomenon is likely due to the fact that HA normally contains a variety of reductive functional groups, including substituted phenols, α-hydroxyl carboxylic acids, oxalic acid and α-carbonyl carboxylic acids, which are capable of reducing high-valence metals, with previous studies showing that NOM can reduce Cr(VI) (Elovitz and Fish, 1995; Jiang et al., 2014), Pu(V) (André and Choppin Gregory, 2000), Vanadium(V) (Wilson and Weber, 1979) and Np(V) (Zeh et al., 1999), to lower valence species. The reduction of W(VI) to W(V) at iron (hydr) oxide organomineral surfaces could significantly change the stability and thus the mobility properties of tungsten in natural environments, compared to that predicted using pure iron (hydr)oxide adsorbents. Although the humic acid sample used in this study may not be representative of all natural NOM, general rules on the effects of

NOM on tungsten adsorption, speciation and resulting mobility are still highly applicable because both humic acid and NOM are known to be abundant in similar O-containing functional groups. Hence, our results indicate that NOM can facilitate the mobility of dissolved tungsten oxyanionic species, especially at acidic to mildly acidic pH, and can promote the reduction of adsorbed tungstate to lower valence species, which likely have different affinity for the organomineral surfaces and thus may similarly contribute to tungsten mobility in soils, sediments and aquatic systems. Overall, both NOM and iron (hydr)oxides coated with NOM should be considered in the prediction of tungsten mobility in the environment.

5. Conclusions

In this study, we examine the adsorption of W(VI) on ferrihydrite in the absence and presence of HA over a range of environmentally relevant W(VI) concentrations, ferrihydrite-HA organomineral couplings and pH values. Results reveal HA inhibits W(VI) uptake to ferrihydrite, with increasing inhibition observed with increasing HA association with the ferrihydrite surfaces, and in particular at acidic to mildly acidic pH. Kinetic results reveal that the adsorption rate of W(VI) on ferrihydrite is decreased in the presence of HA. XPS analysis confirms the formation of W surface complexes on both the ferrihydrite and HA fraction of the organominerals and the presence of HA reduces a significant fraction (~40%) of adsorbed W(VI) to lower valence W(V). Poly tungstate species are observed on ferrihydrite and ferrihydrite organomineral surfaces, particularly at lower pH and in the presence of HA. The adsorption of W(VI) to ferrihydrite and ferrihydrite-HA composite is an energetically favourable process both in terms of the exothermic heat exchange and increase in entropy experienced during adsorption. The results presented here reveal that natural organic matter is a key factor influencing the sequestration and speciation (oxidation state) of tungstate at natural iron (hydr)oxide surfaces, and therefore that organomineral composites, in addition to pure mineral phases, must be considered when modeling tungsten mobility and fate in natural environments.

Acknowledgements

We acknowledge the National Natural Science Foundation of China (41907015), China Postdoctoral Science Foundation (2019M662782), Scientific Research Fund of Hunan Provincial Education Department, China (18B120), and the Royal Society Newton Mobility Grant (No. IE151033) for financial support. We acknowledge the help from Prof. Qiaoyun Huang, Chenchen Qu, Mingkai Ma and Ding Liang (Huazhong Agricultural University) for ITC.

References

André, C., Choppin Gregory, R., 2000. Reduction of Pu(V) by humic acid. Radiochim. Acta, 88, 613-618.

Bostick, B.C.. Sun, J., Landis, J.D., Clausen, J.L., 2018. Tungsten speciation and solubility in munitions-impacted soils. Environ. Sci. Technol. 52, 1045-1053.

Cao, Y., Guo, Q., Shu, Z., Jiao, C., Luo, L., Guo, W., Zhao, Q., Yin, Z., 2019. Tungstate removal from aqueous solution by nanocrystalline iowaite: An iron-bearing layered double hydroxide. Environ. Pollut. 247, 118-127.

Clausen, J.L., Bostick, B.C., Bednar, A.J., Sun, J., Landis, J.D., 2011. Tungsten speciation in firing range soils. ERDC TR-11-1. US Army Corps of Engineers, Environmental Research and Development Center.

Chen, C., Dynes, J.J., Wang, J., Sparks, D.L., 2014. Properties of Fe-organic matter associations via coprecipitation versus adsorption. Environ. Sci. Technol. 48, 13751-13759.

Clausen, J.L., Korte, N., 2009. Environmental fate of tungsten from military use. Sci. Total Environ. 407, 2887-2893.

Cui, M., Johannesson, K.H., 2017. Comparison of tungstate and tetrathiotungstate adsorption onto pyrite. Chem. Geol. 464, 57-68.

Datta, S., Vero, S.E., Hettiarachchi, G.M., Johannesson, K., 2017. Tungsten Contamination of Soils and Sediments: Current State of Science. Current Pollution Reports 3, 55-64.

Davantès, A., Costa, D., Sallman, B., Rakshit, S., Lefèvre, G. 2016. Surface polymerization of Mo(VI) and W(VI) snions on hematite tevealed by in situ infrared spectroscopy and DFT+U theoretical study. J.Phys. Chem. C, 121, 324-332.

Davis, J.A., 1982. Adsorption of natural dissolved organic matter at the oxide/water interface. Geochim. Cosmochim. Acta 46, 2381-2393.

Dermatas, D., Braida, W., Christodoulatos, C., Strigul, N., Panikov, N., Los, M., Larson, S., 2004. Solubility, sorption, and soil respiration effects of tungsten and tungsten alloys. Environ. Forensics 5, 5-13.

Du, H., Chen, W., Cai, P., Rong, X., Chen, C., Huang, Q., 2016. Cadmium adsorption on bacteria–mineral mixtures: effect of naturally occurring ligands. Eur. J. Soil Sci. 67, 641-649.

Du, H.H., Lin, Y.P., Chen, W.L., Cai, P., Rong, X.M., Shi, Z.H., Huang, Q.Y., 2017. Copper adsorption on composites of goethite, cells of *Pseudomonas putida* and humic acid. Eur. J. Soil Sci. 68, 514-523.

Du, H., Huang, Q., Lei, M., Tie, B., 2018a. Sorption of Pb(II) by nanosized ferrihydrite organo-mineral composites formed by adsorption versus coprecipitation. ACS Earth Space Chem. 2, 556-564

Du, H., Peacock, C.L., Chen, W., Huang, Q., 2018b. Binding of Cd by ferrihydrite organo-mineral composites: Implications for Cd mobility and fate in natural and contaminated environments. Chemosphere 207, 404-412.

Du, H., Huang, Q., Zhou, M., Tie, B., Lei, M., Wei, X., Liu, X., Yang, Y., 2018c. Sorption of Cu(II) by Al hydroxide organo–mineral coprecipitates: Microcalorimetry and NanoSIMS observations. Chem. Geolo. 499, 165-171.

Du, H., Qu, C., Ma, M., Lei, M., Tie, B., Liu, X., Wei, X.,Yang, Y., 2019. Insights into Pb(II) binding by Fe/Al hydroxide–microbe composite: XAFS spectroscopy and isothermal titration calorimetry study. Chem. Geolo. 510, 84-90.

Elovitz, M.S., Fish, W., 1995. Redox Interactions of Cr(VI) and substituted phenols: Products and mechanism. Environ. Sci. Technol. 29, 1933-1943.

Fariña, A.O., Peacock, C.L., Fiol, S., Antelo, J., Carvin, B., 2018. A universal adsorption behaviour for Cu uptake by iron (hydr)oxide organo-mineral composites. Chem. Geol. 479, 22-35.

Flynn, E.D., Catalano, J.G., 2017. Competitive and cooperative effects during nickel adsorption to iron oxides in the presence of oxalate. Environ. Sci. Technol. 51, 9792-9799.

Freire, E., Mayorga, O.L., Straume, M., 1990. Isothermal titiration calorimetry. Anal. Chem. 62, 950A-959A.

Gorman-Lewis, D., Fein, J.B., Jensen, M.P., 2006. Enthalpies and entropies of proton and cadmium adsorption onto *Bacillus subtilis* bacterial cells from calorimetric measurements. Geochim. Cosmochim. Acta. 70, 4862-4873.

Gu, B., Schmitt, J., Chen, Z., Liang, L., McCarthy, J.F., 1994. Adsorption and desorption of natural organic matter on iron oxide: mechanisms and models. Environ. Sci. Technol. 28, 38-46.

Gustafsson, J.P., 2003. Modelling molybdate and tungstate adsorption to ferrihydrite. Chem. Geol. 200, 105-115.

Hur, H., Reeder, R.J., 2016. Tungstate sorption mechanisms on boehmite: Systematic uptake studies and X-ray absorption spectroscopy analysis. J. Colloid Interf. Sci. 461, 249-260.

Hur, H., Reeder, R.J., 2018. Formation of CoAl layered double hydroxide on the boehmite surface and its role in tungstate sorption. J. Environ. Sci. 61, 103-115.

Iwai, T., Hashimoto, Y., 2017. Adsorption of tungstate (WO_4) on birnessite, ferrihydrite, gibbsite, goethite and montmorillonite as affected by pH and competitive phosphate (PO_4) and molybdate (MoO_4) oxyanions. Appl. Clay Sci. 143, 372-377.

Jiang, W., Cai, Q., Xu, W., Yang, M., Cai, Y., Dionysiou, D.D., O’Shea, K.E., 2014. Cr(VI) adsorption and reduction by humic acid coated on magnetite. Environ. Sci. Technol. 48, 8078-8085.

Johannesson, K.H., Dave, H.B., Mohajerin, T.J., Datta, S., 2013. Controls on tungsten concentrations in groundwater flow systems: The role of adsorption, aquifer sediment Fe(III) oxide/oxyhydroxide content, and thiotungstate formation. Chem. Geol. 351, 76-94.

Kennedy, A.J., Johnson, D.R., Seiter, J.M., Lindsay, J.H., Boyd, R.E., Bednar, A.J., Allison, P.G., 2012. Tungsten toxicity, bioaccumulation, and compartmentalization into organisms representing two trophic levels. Environ. Sci. Technol. 46, 9646-9652.

Kleber, M., Eusterhues, K., Keiluweit, M., Mikutta, C., Mikutta, R., Nico, P.S., 2015. Mineral–organic associations: Formation, properties, and relevance in soil Environments. Adv. Agron. 130, 1-140.

Koutsospyros, A., Braida, W., Christodoulatos, C., Dermatas, D., Strigul, N., 2006. A review of tungsten: From environmental obscurity to scrutiny. J. Hazard. Mater. 136, 1-19.

Liang, P., Li, Y.C., Zhang, C., Wu, S.C., Cui, H.J., Yu, S., Wong, M.H., 2013. Effects of salinity and humic acid on the sorption of Hg on Fe and Mn hydroxides. J. Hazard. Mater. 244-245, 322-328.

Lindsay, J.H., Kennedy, A.J., Seiter-Moser, J.M., Bednar, A.J., Boyd, R.E., Johnson, D.R., Allison, P., Tappero, R.V., 2017. Uptake kinetics and trophic transfer of tungsten from cabbage to a herbivorous animal model. Environ. Sci. Technol. 51, 13755-13762.

Mikutta, R., Lorenz, D., Guggenberger, G., Haumaier, L., Freund, A., 2014. Properties and reactivity of Fe-organic matter associations formed by coprecipitation versus adsorption: Clues from arsenate batch adsorption. Geochim. Cosmochim. Acta. 144, 258-276.

Mohajerin, T.J., Neal, A.W., Telfeyan, K., Sasihharan, S.M., Ford, S., Yang, N., Chevis, D.A., Grimm, D.A., Datta, S., White, C.D., Johannesson, K.H., 2014a. Geochemistry of tungsten and arsenic in aquifer systems: A comparative study of groundwaters from West Bengal, India, and Nevada, USA. Water Air Soil Pollution, 225, 1792.

Mohajerin T.J., Helz G.R., White C.D., Johannesson K.H., 2014b. Tungsten speciation in sulfidic waters: Determination of thiotungstate formation constants and modeling their distribution in natural waters. Geochim. Cosmochim. Acta 144, 157-172.

Moon, E.M., Peacock, C.L., 2012. Adsorption of Cu(II) to ferrihydrite and ferrihydrite–bacteria composites: Importance of the carboxyl group for Cu mobility in natural environments. Geochim. Cosmochim. Acta 92, 203–219.

Murphy, E.M., Zachara, J.M., Smith, S.C., Phillips, J.L., 1992. The sorption of humic acids to mineral surfaces and their role in contaminant binding. Sci. Total Environ.

117-118, 413-423.

Nancollas, G.H., 1970. The thermodynamics of metal-complex and ion-pair formation. Coordin. Chem. Rev. 5, 379-415.

Oburger, E., Vergara Cid, C., Preiner, J., Hu, J., Hann, S., 2018. pH-dependent bioavailability, speciation, and phytotoxicity of Tungsten (W) in soil affect growth and molybdoenzyme activity of nodulated soybeans. Environ. Sci. Technol. 52, 6146-6156.

Oren, A., Chefetz, B., 2012. Sorptive and desorptive fractionation of dissolved organic matter by mineral soil matrices. J. Environ.l Qual. 41, 526-533.

Otero-Fariña, A., Fiol, S., Arce, F., Antelo, J., 2017. Effects of natural organic matter on the binding of arsenate and copper onto goethite. Chem.Geol. 459, 119-128.

Rakshit, S., Sallman, B., Davantés, A., Lefèvre, G., 2017. Tungstate (VI) sorption on hematite: An in situ ATR-FTIR probe on the mechanism. Chemosphere 168, 685-691.

Sallman, B., Rakshit, S., Lefèvre, G., 2018. Influence of phosphate on tungstate sorption on hematite: A macroscopic and spectroscopic evaluation of the mechanism. Chemosphere 213, 596-601.

Schild, D., Marquardt Christian, M., 2000. Analysis of Th(IV)-humate by XPS. Radiochim. Acta, 88, 587-592.

Schwertmann, U., Fechter, H., 1982, The point of zero charge of natural and synthetic ferrihydrites and its relation to adsorbed silicate. Clay Miner. 17, 471-476.

Seda, N.N., Koenigsmark, F., Vadas, T.M., 2016. Sorption and coprecipitation of copper to ferrihydrite and humic acid organomineral complexes and controls on copper availability. Chemosphere 147, 272-278.

Sparks, D.L., 2002. Environmental Soil Chemistry. Academic Press, New York.

Sposito, G., 1984. The surface chemistry of soils. Oxford University Press.

Strigul, N., Galdun, C., Vaccari, L., Ryan, T., Braida, W., Christodoulatos, C., 2009. Influence of speciation on tungsten toxicity. Desalination 248, 869-879.

Strigul, N., 2010. Does speciation matter for tungsten ecotoxicology? Ecotox. Environ. Safe. 73, 1099-1113.

Sun, J., Bostick, B.C., 2015. Effects of tungstate polymerization on tungsten(VI) adsorption on ferrihydrite. Chem. Geol. 417, 21-31.

Tribalis, A., Panagiotou, G.D., Tsilomelekis, G., Kalampounias, A.G., Bourikas, K., Kordulis, C., Boghosian, S., Lycourghiotis, A., 2014. J. Phys. Chem. C 118, 11319-11332.

Tuna, G.S., Braida, W., Ogundipe, A., Strickland, D., 2012. Assessing tungsten transport in the vadose zone: From dissolution studies to soil columns. Chemosphere 86, 1001-1007.

Wang, Y., Michel, F.M., Choi, Y., Eng, P.J., Levard, C., Siebner, H., Gu, B., Bargar, J.R., Brown, G.E., 2016. Pb, Cu, and Zn distributions at humic acid-coated metal-oxide surfaces. Geochim. Cosmochim. Acta 188, 407-423.

Wilson, S.A., Weber, J.H., 1979. An EPR study of the reduction of vanadium(V) to vanadium(IV) by fulvic acid. Chem. Geol. 26, 345-354.

Woodward, G.L, Peacock, C.L, Otero-Fariña, A., Thompson, O.R., Brown, A.P., Burke, I.T., 2018. A universal uptake mechanism for cobalt(II) on soil constituents: ferrihydrite, kaolinite, humic acid, and organo-mineral composites. Geochim. Cosmochim. Acta 238, 270-291.

Xie, F. Y., Gong, L., Liu, X., Tao, Y.T., Zhang, W.H., Chen, S.H., Meng, H., Chen, J., 2012. XPS studies on surface reduction of tungsten oxide nanowire film by Ar+ bombardment. J. Electron Spectrosc. 185, 112-118.

Xue, Q., Ran, Y., Tan, Y., Peacock, C.L., Du, H., 2019. Arsenite and arsenate binding to ferrihydrite organo-mineral coprecipitate: Implications for arsenic mobility and fate in natural environments. Chemosphere 224, 103-110.

Yan, L., Song, J., Chan, T., Jing, C., 2017. Insights into Antimony Adsorption on {001} TiO2: XAFS and DFT Study. Environ. Sci. Technol. 51, 6335-6341.

Yang, Y., Jia, J., Liu, Y., Zhang, P., 2018. The effect of tungsten doping on the catalytic activity of α-MnO_2 nanomaterial for ozone decomposition under humid condition. Appl. Catal. A-GEN. 562, 132-141.

Zeh, P., Kim, J.I., Marquardt, C.M., Artinger, R., 1999. The reduction of Np(V) in groundwater rich in humic substances. Radiochim. Acta 87, 23-28.

Zhu, J., Pigna, M., Cozzolino, V., Caporale, A.G., Violante, A., 2011. Sorption of arsenite and arsenate on ferrihydrite: effect of organic and inorganic ligands. J. hazard. Mater. 189, 564-571.

Table 1. Adsorption calorimetry parameters for W(VI) adsorption on ferrihydrite (Fh) and ferrihydrite-HA composites at pH 6.5 and 0.01 M ionic strength.

	ΔG (kJ/mol)	ΔH (kJ/mol)	ΔS (J/mol/K)	K_a (M^{-1})
Fh	-20.64	-16.1	15.08	380
FhHA_5 wt.% C	-14.31	-10.12	13.93	312
FhHA_15 wt.% C	-19.33	-15.43	12.96	226

Figure Caption

Figure 1. W(VI) adsorption edges (pH 4-11) on ferrihydrite (Fh) and ferrihydrite-HA composites (FhHA, 5 wt.%C and 15 wt.%C) at 0.01 M ionic strength.

Figure 2. W(VI) adsorption isotherms on ferrihydrite (Fh) and ferrihydrite-HA composites (FhHA, 5 wt.%C and 15 wt.%C) at pH 6.5 and 0.01 M ionic strength. Lines are Langmuir fits.

Figure 3. O (1s) XPS spectra of ferrihydrite and ferrihydrite-HA composite (FhHA_15% C) before and after the binding of W(VI). The blue, red and green lines represent different O species at energies of ~529.9, 531.2 and 532.6 eV, respectively. The corresponding percentages (%) are shown in the brackets.

Figure 4. Tungsten (4f, 5p) XPS spectra of ferrihydrite and ferrihydrite-HA composite (FhHA_15% C) before and after the binding of W(VI). The red spectrum in the range 34.5-36.5 eV is divided into $W^{5+}4f_{7/2}$ and $W^{6+}4f_{7/2}$.

Figure 5. ATR-FTIR spectra of sorbed W(VI) on ferrihydrite and ferrihydrite-HA composite (FhHA_15% C) at fixed ionic strength (0.01 M NaCl) and varying pH values of 4.5, 6.5 and 8.5.

Figure 6. Isothermal titration calorimetry for W(VI) binding to ferrihydrite and ferrihydrite-HA composites (FhHA, 5 wt.%C and 15 wt.%C). The upper panels represent the raw heat flow (μW) *versus* time (s); the lower panels are the heat exchange (μJ) *versus* per titration, each heat exchange is the integral heat of each peak in the upper panels; solid lines are the independent model fits.

Fig. 1

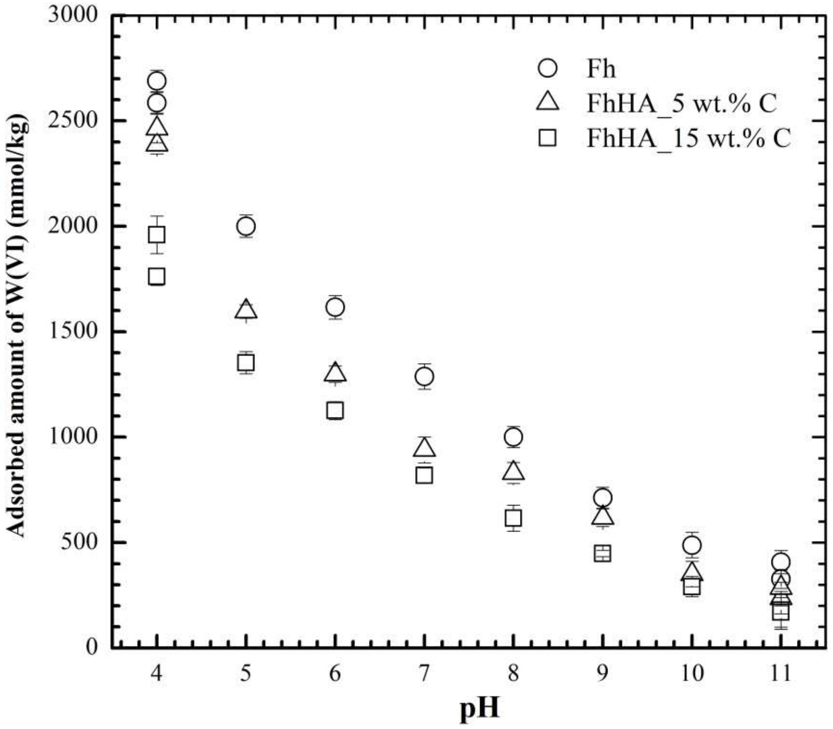
Adsorbed amount of W(VI) (mmol/kg)
pH
0
500
1000
1500
2000
2500
3000
4
5
6
7
8
9
10
11
Fh
FhHA_5 wt.% C
FhHA_15 wt.% C

Fig. 2

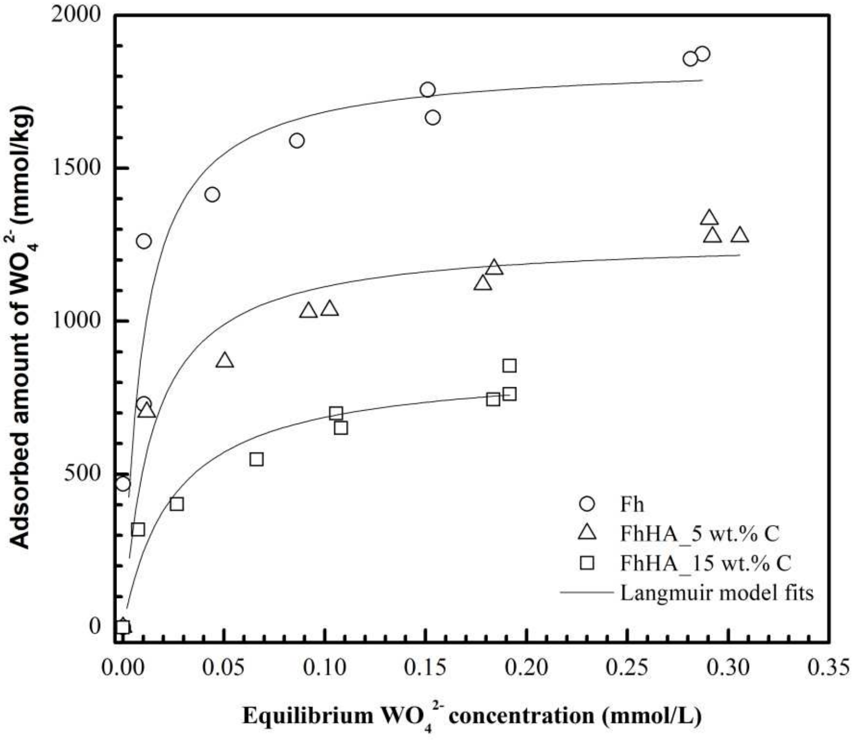
Adsorbed amount of WO_4^{2-} (mmol/kg)
Equilibrium WO_4^{2-} concentration (mmol/L)
0
500
1000
1500
2000
0.00
0.05
0.10
0.15
0.20
0.25
0.30
0.35
Fh
FhHA_5 wt.% C
FhHA_15 wt.% C
Langmuir model fits

Fig. 3

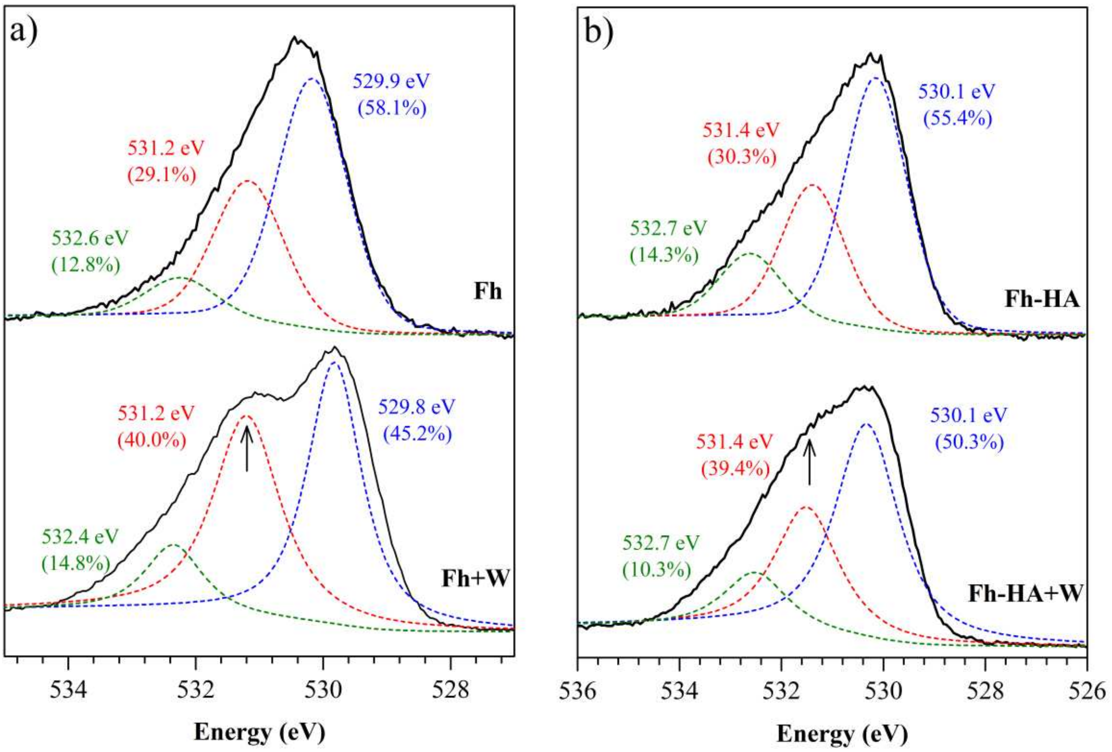
a)
529.9 eV
(58.1%)
531.2 eV
(29.1%)
532.6 eV
(12.8%)
Fh
531.2 eV
(40.0%)
529.8 eV
(45.2%)
532.4 eV
(14.8%)
Fh+W
534
532
530
528
Energy (eV)
b)
530.1 eV
(55.4%)
531.4 eV
(30.3%)
532.7 eV
(14.3%)
Fh-HA
530.1 eV
(50.3%)
531.4 eV
(39.4%)
532.7 eV
(10.3%)
Fh-HA+W
536
534
532
530
528
526
Energy (eV)

Fig. 4

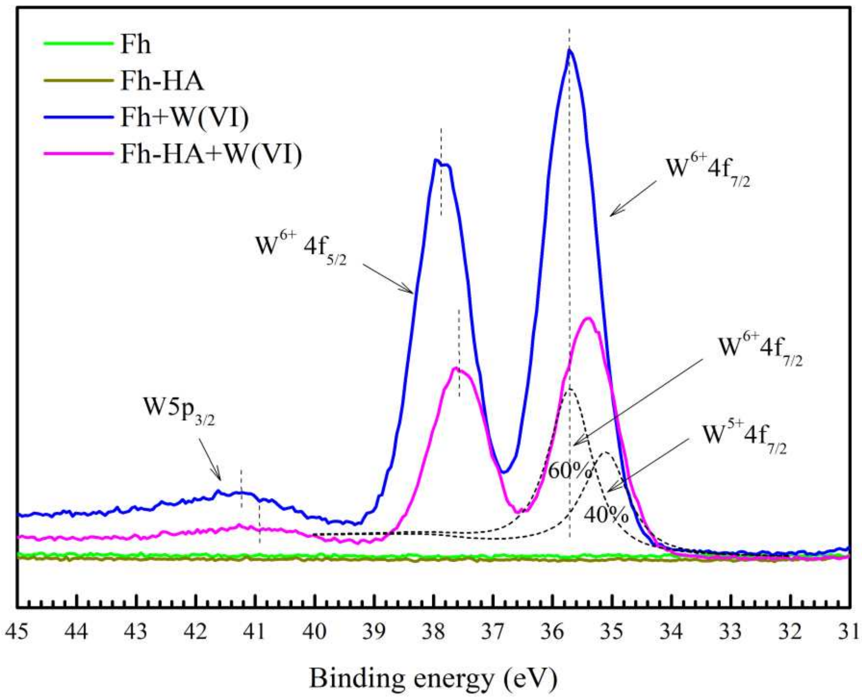
Fh
Fh-HA
Fh+W(VI)
Fh-HA+W(VI)
W^{6+}4f$_{7/2}$
W^{6+} 4f$_{5/2}$
W^{6+}4f$_{7/2}$
W^{5+}4f$_{7/2}$
W5p$_{3/2}$
60%
40%
45
44
43
42
41
40
39
38
37
36
35
34
33
32
31
Binding energy (eV)

Fig. 5

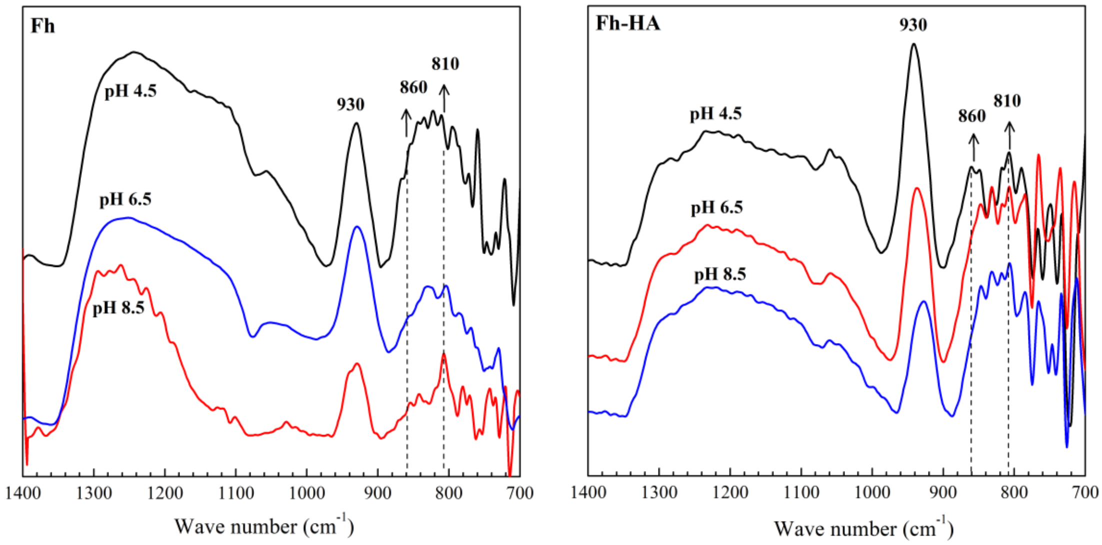

Fig. 6

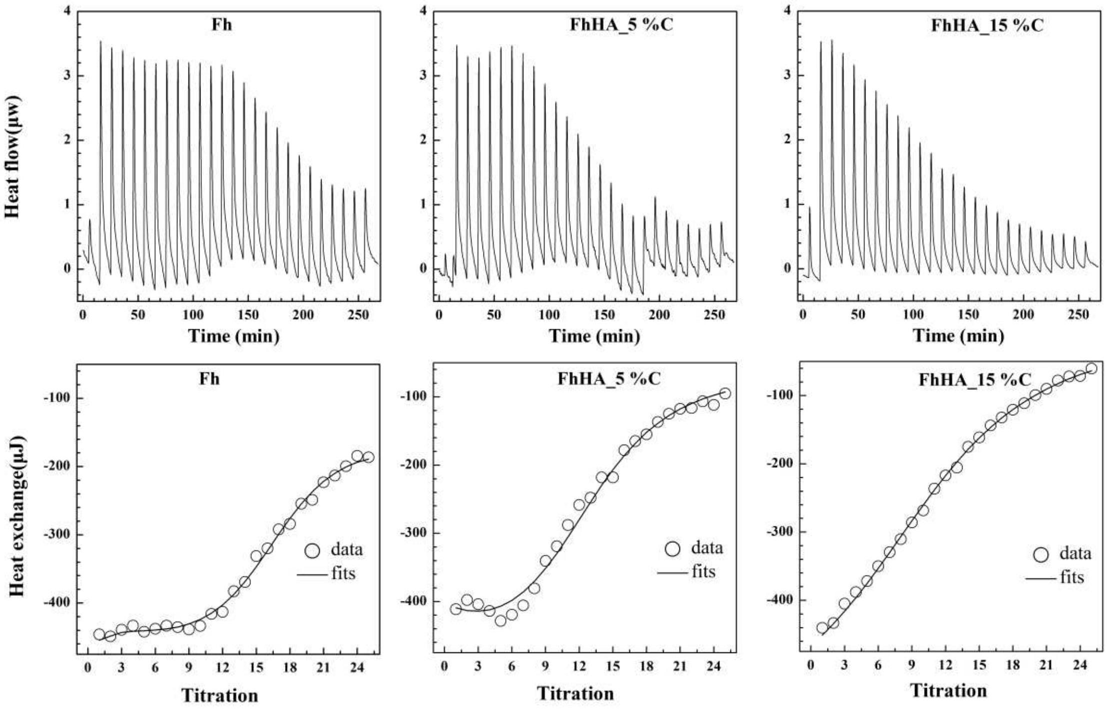

Graphical Abstract

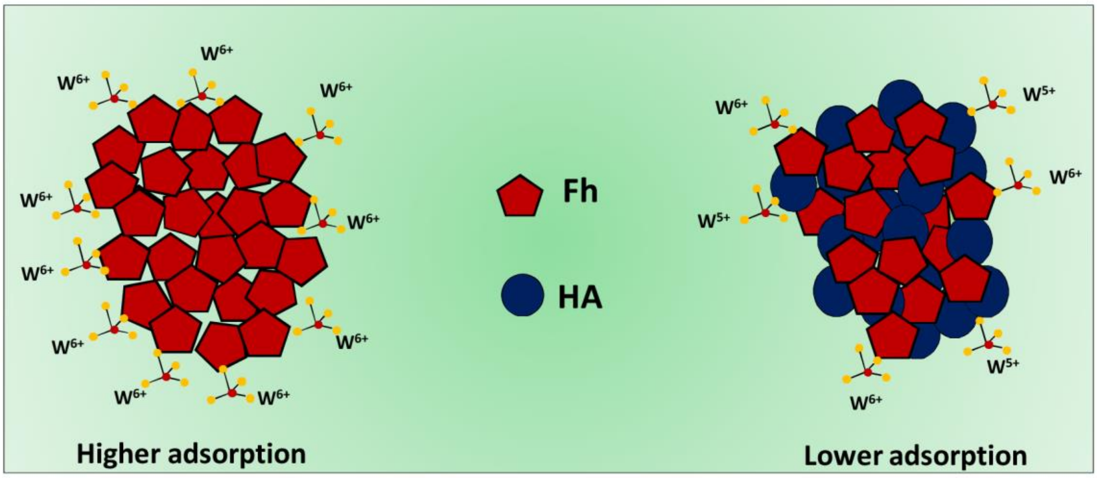
W6+
W5+
Fh
HA
Higher adsorption
Lower adsorption